Available online at www.sciencedirect.com
SCIENCE DIRECT®
Journal of Solid State Chemistry 178 (2005) 2798–2803
JOURNAL OF SOLID STATE CHEMISTRY
www.elsevier.com/locate/jssc

Preparation and characterization of shuttle-like α-Fe_2O_3 nanoparticles by supermolecular template

Xian-Ming Liu[a,b], Shao-Yun Fu[a,*], Hong-Mei Xiao[a,b], Chuan-Jun Huang[a]

[a]*Technical Institute of Physics and Chemistry, Chinese Academy of Sciences, Beijing 100080, China*
[b]*Graduate School of Chinese Academy of Sciences, Beijing 100039, China*

Received 5 April 2005; received in revised form 10 June 2005; accepted 11 June 2005

Abstract

Shuttle-like α-Fe_2O_3 nanoparticles have been successfully synthesized via a new soft-template route using polyethylene glycol (PEG) as polymer, cetyltrimethylammonium bromide (CTAB) as surfactant and $FeCl_3 \cdot 6H_2O$ as iron source materials. Meanwhile, spherical α-Fe_2O_3 nanoparticles are also fabricated under the similar conditions without surfactant and polymer. The resultant products are characterized by means of thermalgravimetric analysis (TGA), powder X-ray diffraction (XRD), infrared (IR) spectroscopy, transmission electron micrograph (TEM), X-ray photoelectron spectra (XPS) and magnetization measurements. The homogeneous α-Fe_2O_3 nanoparticles with shuttle-like shape have an average length of 120 nm and a mean diameter of about 50 nm in the middle part (an average aspect ratio of about 2.5) whereas spherical α-Fe_2O_3 nanoparticles have a mean particle diameter of about 35 nm. Magnetic hysteresis measurements reveal that shuttle-like α-Fe_2O_3 nanoparticles display normal ferromagnetic behaviors while spherical α-Fe_2O_3 nanoparticles exhibit weak ferromagnetic behaviors at room temperature. The two types of α-Fe_2O_3 exhibit hysteretic features with the remanence and coercivity of 0.156 emu/g and 664 Oe, 0.048 emu/g and 110 Oe, respectively. The higher remanent magnetization and coercivity of shuttle-like α-Fe_2O_3 nanoparticles may be associated with the aspect ratio of α-Fe_2O_3 since shape anisotropy would exert a tremendous influence on their magnetic properties.

Keywords: Hematite; Supermolecular template; Ferromagnetism; Remanence; Coercivity

1. Introduction

Nanostructures have received steadily growing interests because of their special electronic, optical, magnetic, and physicochemical properties superior to their bulk counterparts [1–3]. Iron oxides have been widely used for a long time due to their excellent ferromagnetic properties. Among them, α-Fe_2O_3 is the most researched polymorph existing in nature as the mineral hematite. Hematite has a rhombohedrally centered hexagonal structure of the corundum type with a close-packed oxygen lattice in which two-thirds of the octahedral sites are occupied by Fe (III) ions [4]. Additionally, bulk α-Fe_2O_3 is an antiferromagnetic material with the Néel temperature (950 K) and the Morin transition temperature (263 K). The unusual magnetic behavior of α-Fe_2O_3 has recently been studied extensively [5,6]. As stimulated by both the promising applications of iron oxide and the novel properties of nano-scaled materials, synthesis of α-Fe_2O_3 with nanometer dimension is the subject of considerable topical importance. Nanostructured hematite, such as shuttle-like [7,8], nanowire [9–11], nanorod [12] and nanotube [13] has been reported. However, the magnetic properties of those nanostructures have almost never been discussed. These artificial structures can be manipulated to achieve tailored materials for applications and for exploration of physical phenomena, as the magnetic properties of this kind of materials should differ from those of both individual nanoparticles and bulk materials.

Recently, it has been displayed that polymer–surfactant complexes are promising candidates for the

*Corresponding author. Tel./fax: +86 10 62659040.
E-mail address: syfu@mail.ipc.ac.cn (S.-Y. Fu).

0022-4596/$ - see front matter © 2005 Elsevier Inc. All rights reserved.
doi:10.1016/j.jssc.2005.06.018

synthesis of various nanostructures because their synergic structure is totally different from that of pure surfactant systems or pure water-soluble polymers [14,15]. First, the surfactants associated with the polymer chains form micellar aggregates at a critical association concentration, which is often considerably lower than the critical micellar concentration of the surfactants in the pure water. Second, both the polymer and surfactant can act as stabilizers for the crystals, preventing their direct precipitation and aggregation. In addition, the polymer can help to connect the crystals into loose flocs, through a bridging mechanism [14–16]. Third, the electrostatic interaction, strong hydrophobic interactions and van der Waals force between the surfactant and polymer are advantageous to maintaining the stable structure of the template which plays a critical role in the monodispersity and regular shape of the product [17,18]. For example, CTAB associated with the polymer chains could facilitate the formation of rod-shaped micelles. Cao et al. [19] reported that copper nanorods with a high yield and uniform morphology were prepared using PEG and CTAB as the soft template. Polycrystalline nickel nanowires were synthesized by the same soft-template route under magnetic induction [20]. However, this method has not been used to prepare nanostructured iron oxides though it has been exhibited to have many advantages in synthesis of nanomaterials as shown above.

In this paper, the novel soft-template route has been adapted to synthesize α-Fe_2O_3 nanoparticles. First, the precursor, shuttle-like β-FeOOH, was prepared using $FeCl_3 \cdot 6H_2O$ as iron source material under the control of PEG and CTAB aggregates. Then, shuttle-like α-Fe_2O_3 nanoparticles were obtained by calcination of the as-prepared β-FeOOH. In the meantime, spherical α-Fe_2O_3 nanoparticles were also fabricated without supermolecular template. Finally, a plausible mechanism for the formation of these nanostructures was proposed and the dependence of magnetic properties on the particles morphology was discussed.

2. Experimental

All reagents were analytic grade from Beijing Chemical Reagent Ltd. and were used without further purification. Poly (ethylene glycol) (PEG, average M.W. 10000) was used as the polymer, and cetyltrimethylammonium bromide (CTAB) was used as the surfactant. Manipulations and reactions were carried out in air without the protection of nitrogen or inert gas. In a typical experiment, 1 g PEG, 0.36 g CTAB and 1.0 g $FeCl_3 \cdot 6H_2O$ were dissolved in 100 ml de-ionized water in a flask at room temperature. A yellow color was observed in the solution after strongly stirring for half an hour. A 30-min ultrasound treatment is necessary to ensure that all the reagents are homogeneously dispersed in the solution. The solution was stirred at ambient temperature for several hours, which was advantageous to the interaction of ferric ions within the supermolecular template. Then the temperature was increased to 90–100 °C and 20 ml of 28% ammonia solution was added drop wise into the ferric and polymer–surfactant solution. The solution turned yellow immediately and was allowed to stir for an additional 2 h at this temperature. After being cooled to the room temperature, the yellow precipitate was collected and washed with hot water and absolute alcohol several times to remove the remaining CTAB, PEG and other impurities. It was then dried in air at 80 °C for 8 h. Finally, shuttle-like α-Fe_2O_3 nanoparticles were obtained by calcination of the precipitate at 500 °C for 4 h. For the purpose of comparison, spherical α-Fe_2O_3 nanoparticles without the supermolecular templates were also prepared under the similar conditions.

Thermogravimetry (TG) investigation (TA-5000 apparatus, USA) was performed with samples in platinum crucibles and heating rates of 10 K/min. XRD analysis was carried out on a Rigaku D/max2500 diffractometer at a voltage of 40 kV and a current of 200 mA with Cu-$K\alpha$ radiation ($\lambda = 1.5406$ Å), employing a scanning rate 0.02 °/s in the 2θ ranging from 5 to 80 °. TEM images and the electron diffraction (ED) patterns were recorded on a Hitachi-600 transmission electron microscope (TEM) at an accelerating voltage of 200 kV. The infrared (IR) spectra were recorded on a Bruker Equinox-55 spectrometer on the samples palletized with KBr powder. X-ray photoelectron spectroscopy data were obtained with an ESCALab220i-XL electron spectrometer from VG Scientific using 300 W AlKα radiation. The base pressure was about 3×10^{-9} mbar. Magnetic measurements for the samples in the powder form were carried out at room temperature using a vibrating sample magnetometer (VSM, Lakeshore 7307, USA) with a maximum magnetic field of 10 kOe.

3. Results and discussion

A schematic diagram of the proposed growth mechanism is shown in Fig. 1. The formation of shuttle-like α-Fe_2O_3 nanoparticles involves four primary steps: formation of supermolecular template, nucleation of inner FeOOH nanostructures, washing shuttle-like β-FeOOH nanoparticles and calcination of shuttle-like β-FeOOH to obtain shuttle-like α-Fe_2O_3 nanocrystalline particles. Initially, $FeCl_3 \cdot 6H_2O$, CTAB and PEG are dissolved in deionized water, which results in a clear and homogeneous solution. Since there exist interactions between water-soluble polymer and cationic surfactant [18], the surfactants associating with the polymer chains form micellar aggregates at a rather low concentration.

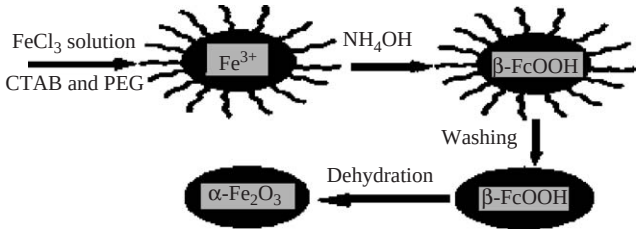

Fig. 1. Schematic representation of the supermolecular-template preparation route of shuttle-like α-Fe_2O_3.

Thus the supermolecular aggregates form in the solution with the coils of PEG chains as the core, around which are the rod-shaped CTAB micelles. Ferric ions react with the supermolecular template under ambient condition. As the solution is heated, ammonia is added and the FeOOH nanostructures nucleate under the control of this template. Then, shuttle-like β-FeOOH nanoparticles are collected and washed to remove the remaining CTAB, PEG and other impurities. Finally, shuttle-like α-Fe_2O_3 nanoparticles can be obtained by calcination of shuttle-like β-FeOOH nanoparticles at 500 °C for 4 h.

The dehydration process of synthetic β-FeOOH was carried out from 30 to 900 °C. The mass decrease of the samples (Fig. 2) is derived from the dehydration of nanostructured β-FeOOH powders. During the whole dehydration process, the total weight loss is 15.30% which is larger than the theoretical value (10.1%), indicating ~5.2% excess hydroxyl units were present in the synthetic β-FeOOH. The powders exhibit thermogravimetric transitions that are likely due to the loss of physisorbed and structural water. The initial weight loss from 30 to 120 °C is attributed to the loss of surface adsorbed water and ethanol. The weight loss in the range of 120–325 °C is due to the removal of the crystalline water molecules, which maintained normally the channels of akaganeite, and the dehydroxylation of the sample akaganeite. After 325 °C, the weight loss continued but gradually slowed at 400 °C and almost ceased at 500 °C. As a consequence, the stable residue can reasonably be ascribed to α-Fe_2O_3.

Fig. 3 shows XRD patterns of the samples. The peaks of the as-prepared FeOOH (Fig. 3A) are in agreement with the theoretical data of the JCPDS card no. 34-1266, indicating the presence of β-FeOOH. However, some impure peaks attributed to α-Fe_2O_3 appear in the XRD pattern of β-FeOOH, indicating that a very small amount of α-Fe_2O_3 impurities might be yielded during the drying process. When β-FeOOH powders were calcined at 500 °C for 2 or 4 h (Fig. 3B), all peaks are in agreement with the theoretical data of hematite (JCPDS card no. 33-0664). It indicates that β-FeOOH powders have completely transformed into hematite. At the moment, the color of samples changes from yellow to red and the XRD peaks become narrow and sharp.

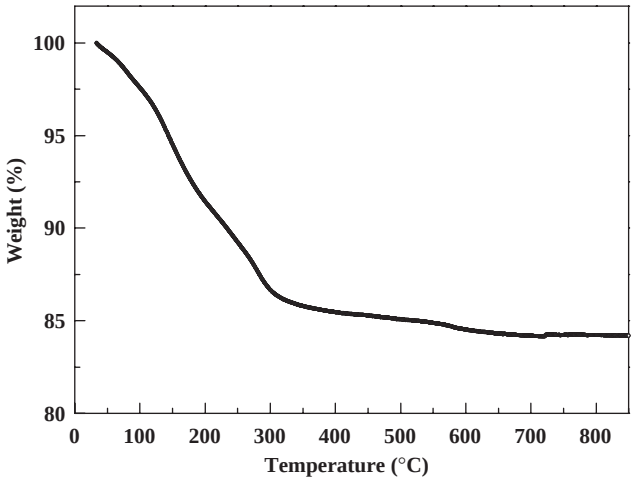

Fig. 2. TG curve of shuttle-like β-FeOOH.

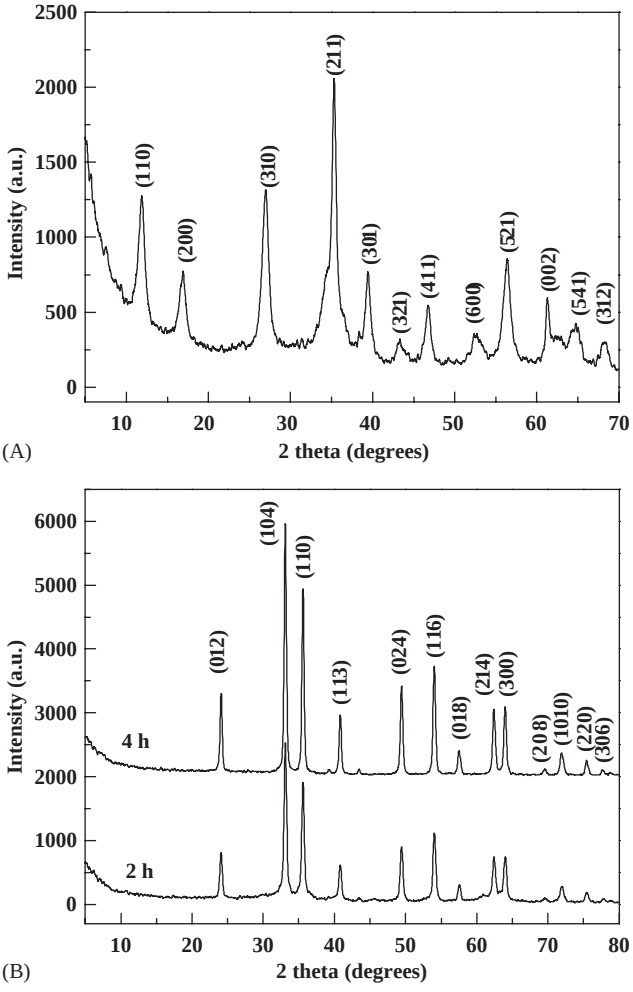

Fig. 3. XRD patterns of the samples. (A) shuttle-like β-FeOOH; (B) shuttle-like α-Fe_2O_3 calcined at 500 °C for 2 and 4 h.

When the thermal transformation is nearly completed and the crystallinity of hematite is improved at 500 °C, the intensity of the (104) peak is larger than that of (110)

peak, which corresponds to the standard XRD pattern of hematite. In addition, the intensity of the peaks increases with the increase of the time.

Fig. 4 shows the morphology of the samples. The morphology of β-FeOOH appears shuttle-like, while α-Fe_2O_3 calcined at 500 °C for 4 h also contains largely shuttle-like nanostructures with an average length of 120 nm and diameter of about 50 nm in the middle part. The results indicate that the existence of the polymer-surfactant can effectively affect the size and shape of ferric oxide nanocrystallites with certain aspect ratio. To further reveal the fine structure of the nanostructured α-Fe_2O_3 shown in Fig. 4C, ED analysis was also carried out. It can be concluded that the shuttle-like materials consist of polycrystals of ferric oxide. It is interesting that some mesopores are developed inside the shuttle-like β-FeOOH nanocrystals (Fig. 4A). When the temperature has reached to 500 °C, the coalescence of the pores and the recrystallization process are still in progress. The size of hematite decreases a little but the shape of hematite almost remains the same as that of the shuttle-like β-FeOOH.

To understand well the effect of the polymer–surfactant on the formation feature of shuttle-like nanoparticles, a synthetic experiment without polymer–surfactant was carried out. It is observed that the spherical nanoparticles were formed; no shuttle-like materials that appeared in the experiment with polymer–surfactant were observed. Fig. 5 shows the images of the spherical samples. The spherical α-Fe_2O_3 nanoparticles are 20–50 nm in diameter. It is found that the dipole magnetic interactions of these nanoparticles in the nanostructures are quite strong. As a rule, the samples must be sonicated continuously for more than half an hour to prepare a sample for TEM observation; however, the nanostructures have not been destroyed, indicating that the polycrystalline nanostructures are rather stable as a result of the soft-template process.

IR spectra of the samples in the range of 4000–400 cm^{-1} are shown in Fig. 6. There is a distinguished adsorption band at 3430 and 1650 cm^{-1}, except three absorbance bands located at 667, 588 and 441 cm^{-1} for β-FeOOH (Fig. 6A). The bands at 3430 and 1650 cm^{-1} were attributed to the stretching vibration and bending vibration adsorption of OH^-, while three absorbance bands at 667, 588 and 441 cm^{-1} were assigned to the absorptions associated with the characteristic Fe–O stretching modes, suggesting that there is only β-FeOOH single phase existing in the system [21]. It gives further evidence of formation of α-Fe_2O_3 phase from Fig. 6B. After β-FeOOH was calcined at 500 °C for 4 h, the bands at 540 and 462 cm^{-1} belong to characteristic bands of polycrystal α-Fe_2O_3 in the IR spectrum [22]. And the intensity of these two peaks was in the order of $540 > 462\ cm^{-1}$. It indicates that α-Fe_2O_3 phase has been formed.

We used XPS to examine the oxidation state of the iron in the products, because core electron lines of ferric ions can be detected in XPS [23,24]. The results of Fe $2p_{3/2}$ and $2p_{1/2}$ electron binding energies are shown in Fig. 7, which are very similar to the values recorded in literature [25]. The binding energies at 711.5 and 725.5 eV are the characteristic doublet from Fe $2p_{3/2}$ and Fe $2p_{1/2}$ core-level electrons, respectively. No other iron signal was detected in the XPS spectra.

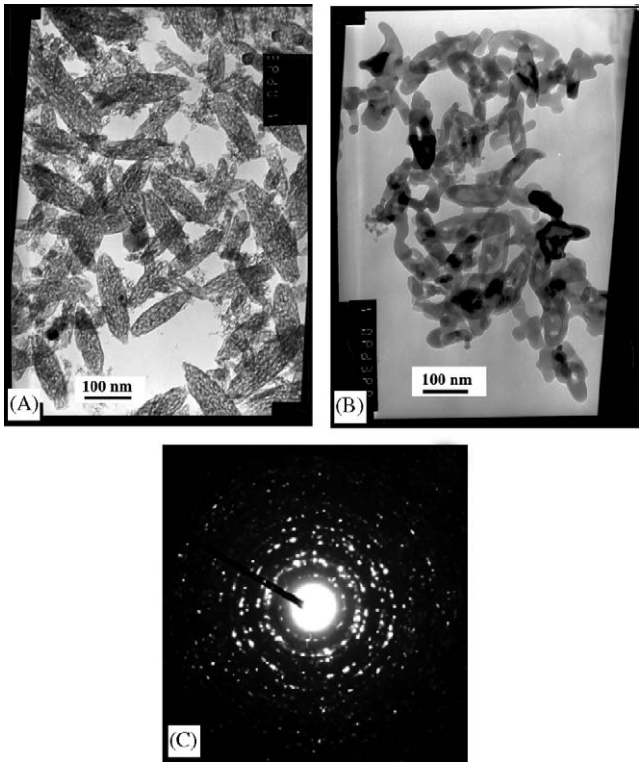

Fig. 4. TEM images and ED pattern of the samples. (A) shuttle-like β-FeOOH; (B) shuttle-like α-Fe_2O_3 calcined at 500 °C for 4 h; (C) ED pattern of shuttle-like α-Fe_2O_3 calcined at 500 °C for 4 h.

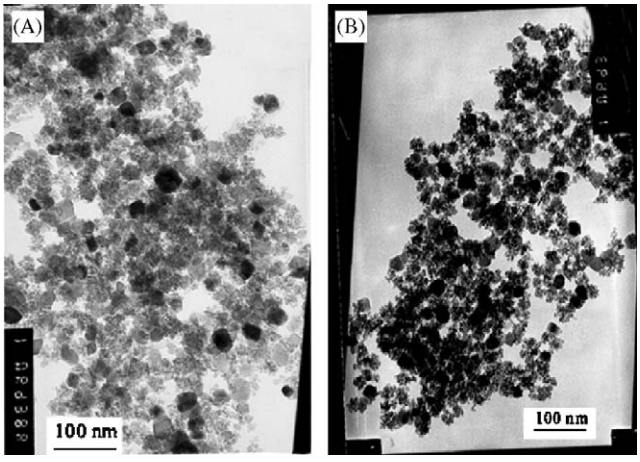

Fig. 5. TEM images of the samples. (A) spherical β-FeOOH; (B) spherical α-Fe_2O_3 calcined at 500 °C for 4 h.

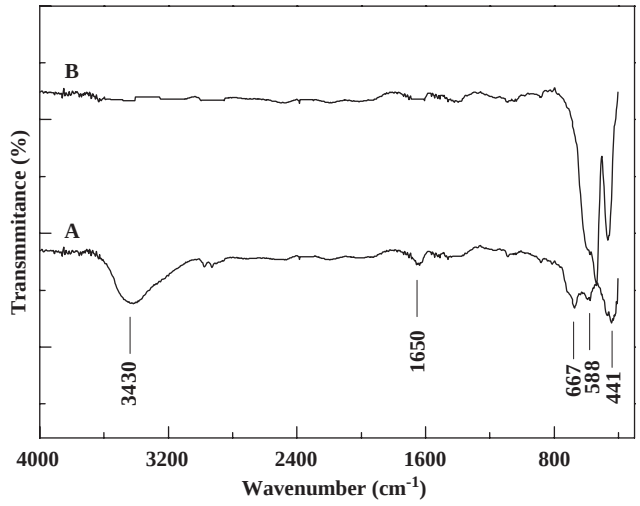

Fig. 6. IR spectra of the samples. (A) shuttle-like β-FeOOH; (B) shuttle-like α-Fe_2O_3 calcined at 500 °C for 4 h.

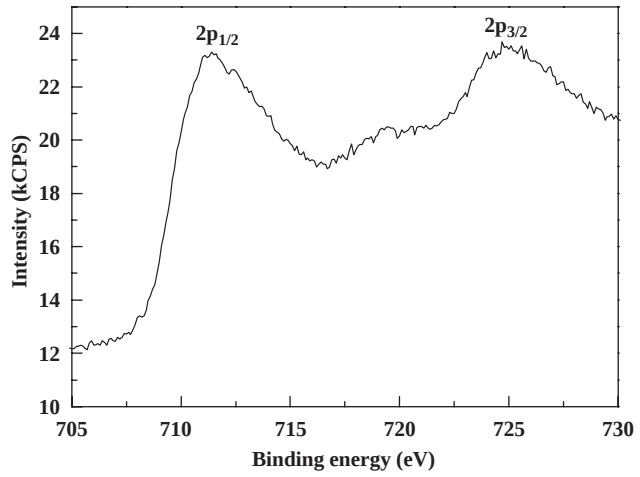

Fig. 7. XPS spectrum of shuttle-like α-Fe_2O_3 calcined at 500 °C for 4 h.

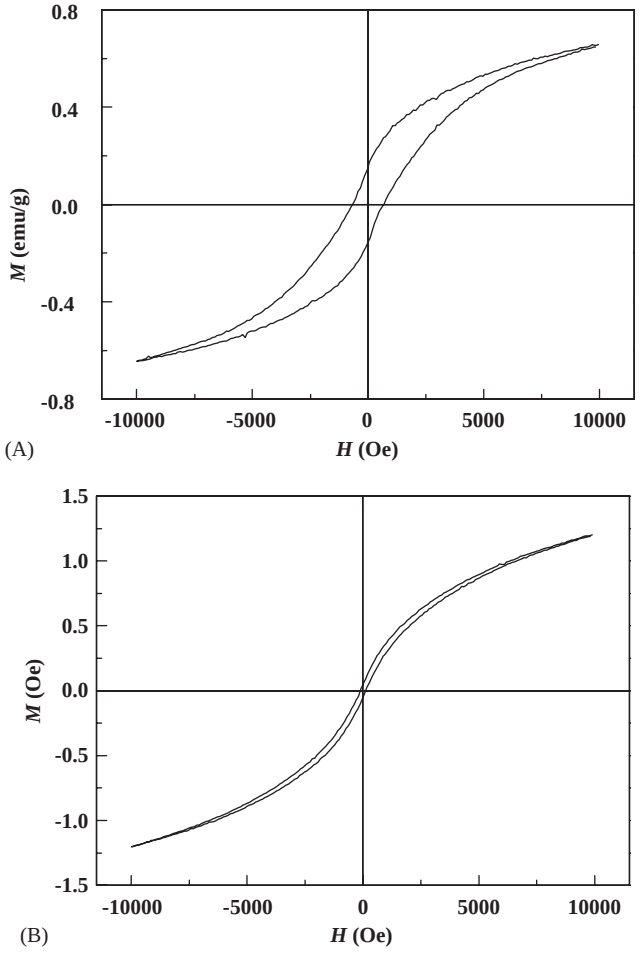

Fig. 8. Hysteresis loops for the samples at room temperature. (A) Shuttle-like α-Fe_2O_3 calcined at 500 °C for 4 h; (B) spherical α-Fe_2O_3 calcined at 500 °C for 4 h.

Magnetic hysteresis maesurements for α-Fe_2O_3 were carried out in applied magnetic field at room temperature, with the field sweeping from −10 to 10 kOe. The hysteresis loops of the samples (see Fig. 8) do not reach saturation up to the maximum applied magnetic field. As shown in Fig. 8, the morphology would affect the magnetic properties of α-Fe_2O_3 nanoparticles. The magnetization measurements of the two type α-Fe_2O_3 exhibit hysteretic feature with the remanent magnetization and coercivity being determined to be 0.156 emu/g and 664 Oe, 0.048 emu/g and 110 Oe, respectively, suggesting that shuttle-like α-Fe_2O_3 nanoparticles are ferromagnetic while spherical α-Fe_2O_3 nanoparticles exhibit weak ferromagnetic behaviors at room temperature. It is found that the high remanent magnetization and coercivity may be associated with the aspect ratio of α-Fe_2O_3 because shape anisotropy would exert a tremendous influence on their magnetic properties. It is well known that the magnetization of ferromagnetic materials is very sensitive to the microstructure of a particular sample [25]. Symmetrically shaped nanoparticles, such as spheres, do not have any net shape anisotropy. However, shuttle-like nanoparticles have shape anisotropy in addition to crystalline anisotropy, which will increase the coercivity. This phenomenon can be explained as follows: since the shuttle-like α-Fe_2O_3 nanoparticles are polycrystalline which consist of large numbers of smaller subparticles inside them. The number of the subparticles increases and changes from the multidomain to single domain, which can result in the enhancement in coercivity. In addition, it is generally accepted that the change on the particle surface can result in the variation in magnetic properties [26,27]. In our case, IR of β-FeOOH (Fig. 6A) clearly shows absorptions due to organic species. For example, around 2950 cm^{-1}, weak C–H absorption can be observed. Thus, it is presumed that the organic residues on the surface of α-Fe_2O_3 nanoparticles may result in the spin pinning owing to the increase of the magnetic surface anisotropy, and then influence the magnetic behaviors.

4. Conclusions

In summary, a new soft-template route has been developed for the preparation of α-Fe_2O_3 nanoparticles. The magnetization measurements of shuttle-like and spherical α-Fe_2O_3 exhibit hysteretic feature with the remanent magnetization and coercivity of 0.156 emu/g and 664 Oe, 0.048 emu/g and 110 Oe, respectively, suggesting that shuttle-like α-Fe_2O_3 nanoparticles show ferromagnetic behaviors while spherical α-Fe_2O_3 nanoparticles exhibit weak ferromagnetic behaviors at room temperature. Thus, it can be concluded that the supermolecular template significantly influences the size and shape of the α-Fe_2O_3 nanoparticles, and thus on their magnetic properties as expected.

Acknowledgment

We appreciate the financial support of the National High Technical Research and Development Program of China (No. 2003AA305890).

References

[1] S.A. Majetich, Y. Jin, Science 284 (1999) 470.
[2] C.B. Murray, C.R. Kagan, M.G. Bawendi, Science 270 (1995) 1335.
[3] A.J. Zarur, J.Y. Ying, Nature 403 (2000) 65.
[4] R. Zboril, M. Mashlan, D. Petridis, Chem. Mater. 14 (2002) 969.
[5] M. Catti, G. Valerio, R. Dovesi, Phys. Rev. B 51 (1995) 7441.
[6] M.F. Hansen, C.B. Koch, S. Mørup, Phys. Rev. B 62 (2000) 1124.
[7] I. ul Haq, E. Matijević, J. Colliod Interf. Sci. 192 (1997) 104.
[8] A.T. Ngo, M.P. Pileni, J. Appl. Phys. 92 (2002) 4649.
[9] C. Pascal, J.L. Pascal, F. Favier, M.L.E. Moubtassim, C. Payen, Chem. Mater. 11 (1999) 141.
[10] Y. Fu, J. Chen, H. Zhang, Chem. Phys. Lett. 350 (2001) 491.
[11] Y. Fu, R. Wang, J. Xu, J. Chen, Y. Yan, A. Narlikar, H. Zhang, Chem. Phys. Lett. 379 (2003) 373.
[12] S. Lian, E. Wang, Z. Kang, Y. Bai, L. Gao, M. Jiang, C. Hu, L. Xu, Solid State Commun. 129 (2004) 485.
[13] X.G. Wen, S.H. Wang, Y. Ding, Z.L. Wang, S.H. Yang, J. Phys. Chem. B 109 (2005) 215.
[14] E. Leontidis, T. Kyprianidou-Leodidou, W. Caseri, P. Robyr, F. Krumeich, K.C. Kyriacou, J. Phys. Chem. B 105 (2001) 4133.
[15] E. Leontidis, T. Kyprianidou-Leodidou, W. Caseri, K.C. Kyriacou, Langmuir 15 (1999) 3381.
[16] S. Stoll, J. Buffle, J. Colloid Interf. Sci. 180 (1996) 548.
[17] J. Philip, T. Jaykumar, P. Kalyanasundaram, B. Raj, O. Mondain-Monval, Phys. Rev. E 66 (2002) 1406.
[18] K. Ballerat-Busserolles, L. Meunier, A.H. Roux, G. Roux-Desgranges, Phys. Chem. Chem. Phys. 3 (2001) 2872.
[19] X.B. Cao, F. Yu, L.Y. Li, Z.Y. Yao, Y. Xie, J. Cryst. Growth 254 (2003) 164.
[20] H.L. Niu, Q.W. Chen, M. Ning, Y.S. Jia, X.J. Wang, J. Phys. Chem. B, 108 (2004) 3996.
[21] T. Sugimoto, A. Muramatsu, J. Colloid Interf. Sci. 184 (1996) 626.
[22] Y. Wang, A. Muramatsu, T. Sugimoto, Colloids Surf. A 134 (1998) 281.
[23] Q. Guo, X. Teng, S. Rahman, H. Yang, J. Am. Chem. Soc. 125 (2003) 630.
[24] T. Fujii, F.M.F. de Groot, G.A. Sawatzky, F.C. Voogt, T. Hibma, K. Okada, Phys. Rev. B 59 (1999) 3195.
[25] M. Sorescu, R.A. Brand, D. Mihaila-Tarabasanu, L. Diamandescu, J. Appl. Phys. 85 (1999) 5546.
[26] Z. Jing, S. Wu, S. Zhang, W. Huang, Mater. Res. Bull. 39 (2004) 2057.
[27] S. Li, H. Bi, B. Cui, F. Zhang, Y. Du, X. Jiang, C. Yang, Q. Yu, Y. Zhu, J. Appl. Phys. 95 (2004) 7420.